Article

The Contribution of Entropy, Enthalpy, and Hydrophobic Desolvation to Cooperativity in Repeat-Protein Folding

Tural Aksel,[1,2] Ananya Majumdar,[3] and Doug Barrick[2,*]
[1]Institute for Multiscale Modeling of Biomolecular Interactions
[2]T.C. Jenkins Department of Biophysics
[3]The Johns Hopkins University Biomolecular NMR Center
Johns Hopkins University, Baltimore, MD 21218, USA
*Correspondence: barrick@jhu.edu
DOI 10.1016/j.str.2010.12.018

SUMMARY

Cooperativity is a defining feature of protein folding, but its thermodynamic and structural origins are not completely understood. By constructing consensus ankyrin repeat protein arrays that have nearly identical sequences, we quantify cooperativity by resolving stability into intrinsic and interfacial components. Heteronuclear NMR and CD spectroscopy show that these constructs adopt ankyrin repeat structures. Applying a one-dimensional Ising model to a series of constructs chosen to maximize information content in unfolding transitions, we quantify stabilities of the terminal capping repeats, and resolve the effects of denaturant into intrinsic and interfacial components. Reversible thermal denaturation resolves interfacial and intrinsic free energies into enthalpic, entropic, and heat capacity terms. Intrinsic folding is entropically disfavored, whereas interfacial interaction is entropically favored and attends a decrease in heat capacity. These results suggest that helix formation and backbone ordering occurs upon intrinsic folding, whereas hydrophobic desolvation occurs upon interfacial interaction, contributing to cooperativity.

INTRODUCTION

Cooperativity is a hallmark of protein folding, involving energetic coupling of elements that are distant in sequence and structure. Despite a long-standing appreciation of the significance of cooperativity in protein folding (Lumry and Biltonen, 1966), experimental studies of cooperativity are typically restricted to a "yes" (the transition is all-or-none) or "no" (the transition has populated intermediates) description. Equilibrium unfolding transitions, induced most often by chemical denaturants or temperature increase, are tested for: (1) a single, sigmoidal transition that can be fitted with a two-state model; (2) coincidence of transitions measured by different probes; and (3) sensitivity coefficients (m-values for chemical denaturation; ΔC_p and ΔH values

for thermal denaturation) that match empirical relations (Myers et al., 1995; Robertson and Murphy, 1997). In favorable cases, van't Hoff (two-state model-dependent) enthalpies can be compared to calorimetric enthalpies. These approaches have shown all-or-none cooperativity to be common in folding of both globular proteins and in many elongated proteins. However, the underlying structural and thermodynamic mechanisms of cooperativity (i.e., quantitative coupling energies and entropies) have remained elusive.

Substantial insight into the cooperativity of the folding transition has come from a marriage of statistical thermodynamics and simplified structural models and energy functions. Lattice models with native-centric energy functions (Go, 1983; Taketomi et al., 1975) show some features of cooperative folding, suggesting that a mismatch between entropy and enthalpy decreases may contribute to a free-energy barrier separating the native and denatured states, a suggestion supported using off-lattice models (Oliveberg and Wolynes, 2005; Onuchic et al., 2000; Thirumalai and Hyeon, 2005; Weinkam et al., 2005). These simplified models suggest plausible sources of cooperativity but cannot quantitatively resolve cooperativity into its energetic and structural components.

Quantitative dissection of protein folding cooperativity requires statistical thermodynamic models that can be used to analyze data directly. Nearest-neighbor or "Ising" models (Ising, 1925; Poland and Scheraga, 1970) have been a staple for analyzing cooperativity in simple linear systems, including the helix-coil transition (Doig, 2002; Poland and Scheraga, 1970; Zimm, 1960), and magnetization in arrays of spins systems (Ising, 1925; Onsager, 1944). These models represent structure with repeating units, and give conformational energy as a sum of intrinsic stabilities of the units and coupling energies between neighboring units. The magnitude of the interfacial coupling energy, along with the instability of individual units, determines the extent of cooperativity of the system as a whole. Although there has been interest in applying these models to globular proteins (Munoz, 2001), the heterogeneity of globular proteins precludes representation in terms of structural units and their intrinsic and interactions energies.

In the last decade, proteins with regular, repetitive structure have become increasingly popular for studies of protein folding (Kloss et al., 2008) and for application of Ising models (Aksel and Barrick, 2009; Kajander et al., 2005; Mello and Barrick,

2004; Wetzel et al., 2008). Analysis of folding energies of a series of overlapping ankyrin repeat constructs (33 residues each) from the *Drosophila* Notch receptor indicates that cooperativity results from stabilizing nearest-neighbor interactions that offset intrinsically unstable repeats, although sequence variation among repeats prevents analysis at the single-repeat level.

Recently, several groups have built and analyzed repeat proteins with greatly reduced sequence variation, thereby enabling more exact thermodynamic models of folding (Kajander et al., 2005; Mosavi et al., 2002; Wetzel et al., 2008). Here, we use a series ankyrin constructs that have nearly identical repeats to give a complete description of folding thermodynamics. The structure of a three-repeat construct matches the target ankyrin fold. Guanidine hydrochloride (GdnHCl) and thermal denaturation of this series are resolved into intrinsic and interfacial energies, providing a quantitative representation of folding cooperativity. Intrinsic and interfacial energies are further resolved into enthalpic and entropic components, as well as GdnHCl sensitivity and heat capacity terms. Both chain entropy decrease and hydrophobic desolvation play a major role in folding cooperativity, which is enhanced by GdnHCl.

RESULTS

Sequence Design
Several laboratories have shown that identical consensus ankyrin repeat proteins (CARPs) require modification of the terminal repeats for high solubility. Pluckthun and coworkers (Wetzel et al., 2008) built soluble, folded CARPs using N- and C-terminal caps from GABP-β, a naturally occurring ankyrin repeat protein, (18 and 17 sequence differences between N- and C-terminal caps and internal repeats). We obtained soluble CARPs by embedding a different consensus sequence within the ankyrin domain of the *Drosophila* Notch receptor (Tripp and Barrick, 2007). Here, we sought to maintain solubility of this consensus sequence using single-repeat "caps" that closely match the consensus sequence. This capping strategy resembles that of Mosavi and Peng (2003), which targeted nonpolar residues on the solvent-exposed face of the terminal repeats. We substituted four nonpolar residues each on the N- and C-terminal repeats with charged or polar residues (Table 1).

To further minimize sequence differences, we characterized constructs with a single capping repeat, either at the N or C terminus. These constructs are essential for resolving stability differences between capping and internal repeats (Aksel and Barrick, 2009). Feasibility of this single-cap approach was suggested from studies of singly capped consensus TPR arrays (Main et al., 2003) and by studies of Notch-consensus fusions (Tripp and Barrick, 2007). To monitor unfolding using fluorescence, we replaced an asn at position five with a trp (Table 1, repeat W). In the hidden Markov model on which the ankyrin consensus sequence is based (Finn et al., 2008), this is the most common position for trp.

Solution Structure of CARPs
CARPs containing single capping repeats at either the N terminus or the C terminus expressed to high levels in *E. coli*, as did doubly capped constructs. Although CARPs partitioned largely to the cell pellet, they could be solubilized, purified, and

Table 1. Ankyrin Consensus Sequence and Variants Used in This Study

	1	6	11	16	21	26	31
	●	●	●	●	●	●	●
Secondary Structure[a]	eeeeeeHHHHHHHeeeHHHHHHHHHeeeeeeee						
N-terminal cap (N)	SKDGNTPLH**N**AAKNGHAE**E**VK**K**LL**S**KGADVNAR						
Consensus repeat (R)	SKDGNTPLHLAAKNGHAEIVKLLLAKGADVNAR						
Consensus trp-substituted repeat (W)	SKDG**W**TPLHLAAKNGHAEIVKLLLAKGADVNAR						
C-terminal cap (C)	SKDGNTP**E**HLA**K**KNGH**H**EIVKLL**D**AKGADVNAR						
	●	●	●	●	●	●	●
	1	6	10	16	21	26	31

Sequence substitutions to capping repeats (N and C) and to introduce a tryptophan at position five (N5W) are shown in bold.

[a] The secondary structure, as determined by TALOS+ (Shen et al., 2009) for the central repeat (R) of NRC, is shown along with the numbering scheme used here (H, helix; e, extended). See Figure S5 for cloning procedures.

highly concentrated. All constructs have α-helical secondary structure, as judged by far-UV CD spectroscopy (Figure 1A). For constructs lacking trp at consensus position five, we find only minor differences in molar residue ellipticity from construct to construct. These differences are no larger than prep-to-prep variation and are likely to result from uncertainties in concentration determination, rather than differences in structure. To compare shapes of CD spectra of different constructs, we scaled spectra from 206 to 222 nm (Figure 1A). For constructs lacking trp substitutions, spectral shapes are nearly identical, indicating a similar secondary structure content. Constructs with trp at position five show a positive CD feature around 230 nm, likely a result of exciton coupling of the trp side chains. Velocity sedimentation studies indicate that constructs containing N-caps are monomeric to concentrations above 100 μM (see Figure S1 available online). For R_4C, we find a weak tendency toward self-association, although at concentrations used here for unfolding studies, only monomeric protein would be populated.

To probe whether these constructs adopt an ankyrin fold, we used NMR to determine the structure of NRC. Although the three repeats have high sequence similarity, the ^1H-^{15}N-HSQC spectrum of NRC shows high dispersion. A total of 126 cross-peaks can be detected, and almost all are baseline resolved (Figure 2A). This is close to the 135 potential cross-peaks expected from primary sequence (113 non-prolyl backbone NHs, two trp side chain NHs, ten asn side chain NH$_2$s).

Using standard 3D NMR methods (Figure S2), we assigned backbone and side chain ^{15}N, ^{13}C, and ^1H resonances, and measured ^1H-^1H NOE intensities. We could assign 104 backbone NH resonances, including all NHs in the ankyrin repeats. Consistent with known ankyrin repeat structures, we find two stretches with measurable H(N),H(N)(i,i+1) and Hα,HN(i,i+3)
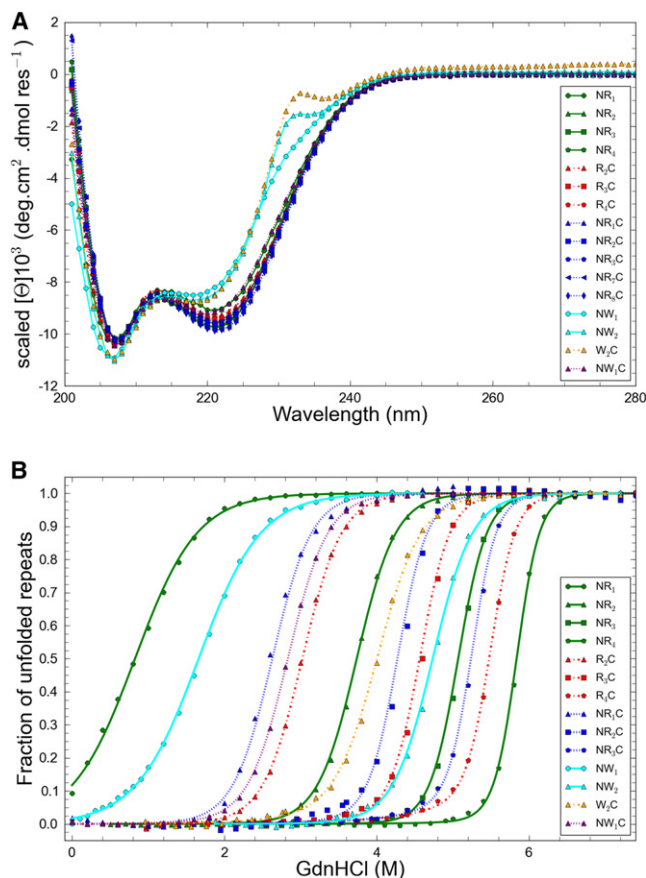
Figure 1. Far UV CD Spectra and GdnHCl-Unfolding Transitions of CARPs

To compare shape (A), spectra are scaled to the same average intensity as NR_2 from 206 to 222 nm. Spectra have similar shapes, except for constructs with trp substitution at position five. (B) GdnHCl titration of CARPs. Constructs are as indicated in the legend. Lines result from global fits of an Ising model to the transitions shown here and to two replicate transitions for each construct (data not shown). Curves are normalized after fitting by subtracting the fitted baselines. Transitions are independent of concentration over the range studied here (see text and Figure S1). Conditions: 150 mM NaCl, 25 mM Tris-HCl (pH 8.0), 20°C.

NOEs, positive $^{13}C_\alpha$ and ^{13}CO chemical shift deviation, and negative $^1H_\alpha$ chemical shift deviation in each repeat (Figure 2B). Inputting chemical shifts into TALOS+ (Shen et al., 2009), two helices are predicted in the same position of each repeat, matching helix locations in known ankyrin repeat proteins.

To determine the structure and relative orientations of the ankyrin repeats of NRC, we generated and refined 20 structural models using short- and long-range ^1H-^1H NOEs (Table 2). To help define relative orientations of the helices with respect to the molecular axis, we included residual dipolar couplings (RDCs) from a partly aligned NRC sample at a late stage of structural refinement. Resulting structures superpose well over the helical regions of the three repeats, with an average backbone rmsd of 1.0 Å (Table 2 and Figure 3) (PDB ID 2L6B). Residues on the N and C termini with significantly higher rmsd are not part of the consensus ankyrin sequence but correspond to cloning sites and the his₆-tag, respectively (Figure 2B).

Measured RDC values, which vary significantly throughout the sequence (but show regular periodicity among repeats) (Figure 2B), are consistent with the resulting structures (Figure 3D). The solution structure of NRC is very similar to other ankyrin repeat proteins (Figures 3A and 3B). As designed, the substitutions in the N- and C-terminal caps are solvent exposed and point away from the central repeat (Figure 3D). Thus, these substitutions are not expected to perturb interaction with neighboring repeats.

To assess dynamic flexibility, we measured R_1 and R_2 values for backbone ^{15}N nuclei, and quantified ^{15}N-^1H NOE intensities. Data were analyzed using ModelFree, and local (residue by residue) motional models were selected based on comparison of χ^2 values, assuming an F distribution (Mandel et al., 1995). We find uniformly low dynamic motion (high-order parameter, S^2) extending from the start of the first helix of the N-cap through the last helix of the C-cap (Figure 4). This includes the two extended recognition loops that connect adjacent repeats (N to R and R to C). The observation that these loops are well ordered in an unbound state (and in a construct defined only by consensus information) suggests that this important recognition element can be rigid on the ps-ns timescale, as was observed in p19^{INK4d} (five repeats) (Renner et al., 1998). The increased motion seen in the binding loops of IκBα (six repeats) (Cervantes et al., 2009) may reflect the greater overall dynamics seen in the unbound state of that particular protein. Not surprisingly, the terminal regions of NRC, which show higher backbone rmsd values, show significantly lower S^2 values, i.e., significantly higher conformational dynamics on the ps-ns timescale.

GdnHCl-Induced Unfolding Transitions of CARPs

To measure CARP stability, the effects of the N- and C-terminal capping substitution, and to resolve stability into intrinsic and nearest-neighbor interaction energies using an Ising model, we monitored GdnHCl-induced unfolding using CD spectroscopy. We have measured unfolding curves on four different series of CARPS of different lengths. One series includes only N-terminal caps (NR to NR_4; two to five repeats, respectively), a second includes only C-terminal caps (R_2C to R_4C, three to five repeats), and a third includes both N- and C-terminal caps (NRC to NR_3C, three to five repeats). In addition a fourth series includes one or more trp-substituted consensus repeats with different capping configurations (NW, NW_2, W_2C, NWC). For R_4C, which shows weak self-association by AUC, unfolding transitions are independent of concentration from 0.6 to 12 μM (Figure S1).

Several general trends emerge from the GdnHCl-unfolding transitions (Figure 1B): (1) all constructs unfold with a single sigmoidal transition; (2) within each series, stability increases with repeat number, as seen by increases in the GdnHCl-unfolding midpoint; (3) the steepness of the transition increases with increasing repeat number; (4) comparing constructs of the same length but different end repeats shows capping repeats to contribute less to stability than internal consensus repeats; (5) of the two caps, the C-terminal caps are least stabilizing, as was seen by Yu et al. (2006); and (6) trp substitution at position five is stabilizing; this unexpected stability enhancement permits a full unfolding transition to be observed for a two-repeat construct (NW), which strongly constrains the fitted values of

Figure 2. NMR Data for a Three-Repeat Consensus Ankyrin Protein

(A) ^{15}N-^{1}H HSQC spectrum of uniformly ^{15}N-labeled NRC at 800 MHz ([pH 6.5] 25°C). For examples of strip plots used for assignment, see Figure S2.

(B) Amide ^{1}H-^{15}N RDCs, short- and medium-range NOEs (normalized to the maximum NOE value of each type), predicted secondary structure from TALOS+ (Shen et al., 2009), and chemical shift deviation from random coil values, calculated using CSI v2.0 (Wishart and Sykes, 1994). Boxed regions of sequence correspond to unstructured regions (horizontal line, Figure 3C). Residues that are helical in the NMR structure, as determined using STRIDE (Heinig and Frishman, 2004), are indicated by spirals.

independent intrinsic folding energy parameters for the N-cap, C-cap, internal consensus repeats, and trp-substituted (W) consensus repeats (ΔG_N, ΔG_C, ΔG_R, ΔG_W). Since substitutions to the N- and C-caps point away from neighboring (R) repeats (Figure 3B), we use a single inter-facial energy for interaction of N, R, and C repeats ($\Delta G_{i,i+1}$; for algebraic reasons, changes in cap stability cannot be resolved into intrinsic versus interfacial terms) (see Equations S2 and S3). However, we expect that substitution of trp at position five may alter contacts with adjacent repeats. Thus, we included separate interfacial energies for W repeats (Table 3).

We model the GdnHCl dependence of stability with two independent terms affecting intrinsic (m_i) and interfacial stability ($m_{i,i+1}$). We assume m_i and $m_{i,i+1}$ to be independent of repeat identity (N, R, W, C). In our initial fitting studies of constructs that contained only combinations of repeats N, R, and C (i.e., no W repeats), we found m_i and $m_{i,i+1}$ to have a strong inverse correlation and, thus, were poorly resolved in the fit. This is because the number of repeats is directly correlated with the number of interfaces, although the two values are offset (i.e., repeats = interfaces + 1). Including W repeats (and the NW construct, with only one interface for two repeats)

intrinsic versus interfacial denaturant dependence in the Ising analysis (see below).

Ising Analysis of GdnHCl-Induced Unfolding Transitions

To determine the intrinsic and nearest-neighbor interaction free energies, we globally fitted an Ising model to the CARP-unfolding transitions in Figure 1B (solid lines). The fitted model includes

decreases the correlation between m_i and $m_{i,i+1}$. The fitted free energies of N, R, and C repeats change very little when W repeats are excluded from the fit (data not shown), indicating that this additional level of parameterization does not compromise fitted free-energy values.

The Ising model can be well fitted to the GdnHCl-unfolding transitions with ten globally shared thermodynamic parameters

Table 2. NRC NMR Solution Structure Statistics

Rmsd Statistics		NOE Distance Constraints	
Number of residues	86 (12–97)[a]	Total	1354
Backbone (Å)	1.00 ± 0.26	Intraresidual (i,i)	327
Heavy atom (Å)	1.92 ± 0.24	Sequential (i,i+1)	358
^{15}N-^{1}H RDC		Short range (i,i+2)	127
Number of constraints	53	Medium range (i,i+3)	175
D_α = 14.06	η = 0.545	Long range (i,i+j;$j \geq i+4$)	367

NMR structure calculation is performed using CYANA via the UNIO interface as described in Supplemental Experimental Procedures. The structure statistics are obtained from the ensemble of 20 models generated at the end of seven successive CYANA runs. N- and C-terminal residues with a low density of NOEs are excluded from rmsd calculations. RDC data were used at a late stage of refinement for further optimization of the models using XPLOR-NIH (Supplemental Experimental Procedures). Axiality (D_α) and rhombicity (η) are calculated from RDC data and the refined structure by XPLOR-NIH.
[a] Residue range used for rmsd calculations.

(Table 3) fitted to 14 well-resolved curves from different constructs (in triplicate), in addition to local baseline parameters for each construct. Uncertainties in fitted parameters were estimated by bootstrap analysis of residuals at the 95% confidence level (Aksel and Barrick, 2009). Uncertainties in fitted free energies are typically quite low (0.1–0.3 kcal/mol, less than 3% of the total parameter value). Uncertainties in fitted m-values are somewhat larger (5% and 18% of the total parameter value for m_i and $m_{i,i+1}$, respectively) but are still low enough to provide insight into the origin of the GdnHCl dependence.

The fitted free energies for intrinsic folding and interfacial interaction are consistent with a high level of global cooperativity observed in the unfolding transitions. The interfacial interactions are all very stabilizing, ranging from −11.5 to −12.5 kcal/mol per interface, in the absence of denaturant and at 20°C (pH 8.0). This strong favorable interaction is offset by an unfavorable intrinsic folding energy, ranging from +3.5 to +7.5 kcal/mol per repeat. This partitioning of free energies rarifies partly folded states: single-folded repeats are strongly disfavored, but when one or more repeats are folded, the folding and subsequent interfacial interaction of nearest-neighbor repeats (with favorable free energy +5.5 − 12 = −6.5 kcal/mol) drives the reaction toward the fully folded state.

As described above, variation in repeat identities allows us to quantify differences in stability between N- and C-terminal capping repeats, and between R and W repeats. Modeled as intrinsic stability differences, the C-terminal capping repeat has the lowest stability of all the repeats, with an intrinsic folding free energy 2.5 kcal/mol higher than the consensus R repeat (Table 3). The N-terminal capping repeat has an intrinsic folding free energy in between the C and R repeats. In contrast the W repeat is more stabilizing than the consensus R repeat by ~1.8 kcal/mol, although interfaces between W repeats are modestly less stabilizing than those between R repeats (0.6–0.8 kcal/mol).

Taking advantage of the constraint provided by W-containing constructs, we find the denaturant sensitivity of intrinsic folding to be twice that of interfacial interaction (Table 3). This observation is consistent with burial of polar backbone surface area in intrinsic folding, which would be expected if the α helices
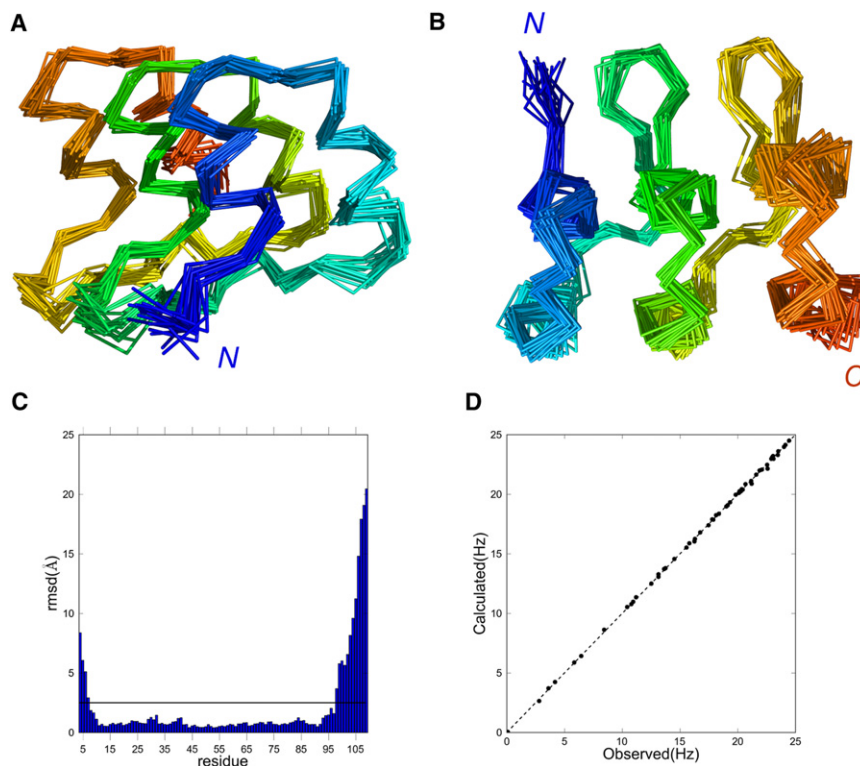
Figure 3. Solution Structure of NRC

(A and B) Cα-traces of 20 models superposed using backbone atoms from residues 12 to 97 in two different views.

(C) Backbone RMSD of the 20 structures in the ensemble. The horizontal line shows the deviation (2.5 Å) selected as a cutoff for structural superposition (A and B) and analysis (Table 2).

(D) Calculated RDC values (averaged from the final structural models) agree well with measured RDC values. Structures are rendered using PyMOL (DeLano, 2003).
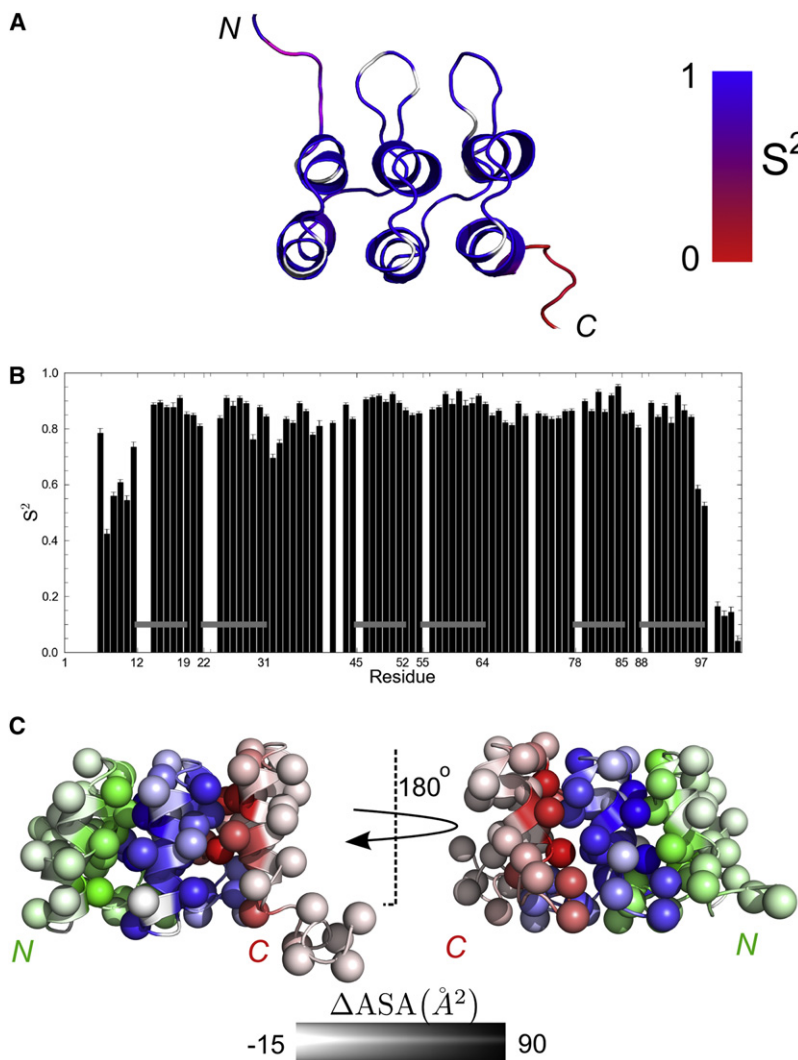
Figure 4. Backbone Dynamics of NRC

(A) Residues in a representative ribbon structure (Figure 3) are coded according to an order parameter S^2 (see text and Table S1). White regions correspond to prolyl residues or to residues that could not be assigned to any local model by the ModelFree approach (Mandel et al., 1995).

(B) S^2 values as a function of sequence. Gray horizontal bars correspond to α helices.

(C) Apolar surface area burial upon formation of interfaces between repeats. For clarity, side chains are represented by spheres centered at C_β. N-cap, R and C-cap repeats are colored by green, blue, and red, respectively. Degree of burial is depicted by color intensity. Burial of interfacial surface area is calculated by subtracting the SASA of the NRC NMR structures from N-cap, R, and C-cap fragments (excised from NRC). Values represent the average from all 20 structures in our ensemble.

interest here) and GdnHCl sensitivities, both for interfacial and intrinsic interactions. In addition, cross-terms are needed to describe the effect of GdnHCl on thermal denaturation. We modeled this coupling as a linear dependence of free energy, entropy, and heat capacity on GdnHCl (Nicholson and Scholtz, 1996). A linear urea dependence for heat capacity of unfolding of the Notch ankyrin domain has been observed (Zweifel and Barrick, 2002). To better determine the effects of GdnHCl on thermal-unfolding parameters, we supplemented the pH 5.0 thermal transitions (Figure 5A) with GdnHCl-unfolding transitions at different temperatures (Figure 5B). Both the thermal- and GdnHCl-induced unfolding transitions were fitted globally (64 curves total) with an Ising model (Figure 5 and Table 4). To further constrain the cross-terms, we fixed the relative GdnHCl sensitivities of intrinsic folding and interfacial interaction to the value found at pH 8.0, 20°C ($m_{i,i+1}/m_i = 0.5$), and also at extreme values ranging from an entirely intrinsic to a largely interfacial GdnHCl effect. We find slightly better fits when the GdnHCl effect is intrinsic, but for the most part the data are well fitted for all ratios explored.

For all $m_{i,i+1}/m_i$ ratios explored, we find the entropy/enthalpy decomposition of the intrinsic folding energy to be opposite to that of the interfacial interaction energy (Table 4). Folding of individual repeats is enthalpically favorable but entropically unfavorable, with entropy making the larger contribution, resulting in an unfavorable intrinsic folding free energy. In contrast the interfacial interaction is enthalpically unfavorable at 20°C, but it is highly stabilized entropically. The heat capacity decrement (ΔC_p, which is negative for protein folding) is partitioned entirely into the interfacial interaction: within the bootstrap error, intrinsic folding of a single repeat has no heat capacity change (Table 4).

DISCUSSION

The motivations of the present study are to better understand cooperativity in protein folding. We measure local and

became ordered in this step. The nonzero interfacial m-value may result from a solubilizing effect of GdnHCl on the interfaces but also likely results from the fact that not all 33 residues of each terminal repeat are folded (Figure 3). Adding a new repeat to the N or C terminus of a folded cluster of repeats would promote folding of the last few residues at the old end of the cluster; the denaturant sensitivity of this coupled folding would show up in the nearest-neighbor term ($m_{i,i+1}$).

Thermal Unfolding of CARPs

With the goal of resolving the free energies of intrinsic folding and interfacial interaction into enthalpy, entropy, and heat capacity changes, we sought conditions in which we could measure complete, reversible thermal-unfolding transitions. Although thermal transitions were neither complete nor fully reversible at pH 8.0, we found that we could obtain full reversibility at pH 5, and by adding low concentrations of GdnHCl (<1.2 M), we could obtain complete unfolding transitions (Figure S3).

Because of the variable amounts of GdnHCl at pH 5.0, Ising analysis of CARP thermal unfolding required both thermal unfolding parameters (ΔH, ΔS, and ΔC_p; parameters of primary

Table 3. Parameters Obtained from GdnHCl Titration Data at pH 8, 20°C

ΔG_N	ΔG_R	ΔG_W	ΔG_C	m_i
6.13 ± 0.17	5.24 ± 0.17	3.40 ± 0.12	7.75 ± 0.19	0.58 ± 0.03
$\Delta G_{R\text{-}R}$	$\Delta G_{W\text{-}W}$	$\Delta G_{N\text{-}W}$	$\Delta G_{W\text{-}C}$	$m_{i,i+1}$
−12.54 ± 0.27	−11.77 ± 0.20	−11.89 ± 0.23	−11.81 ± 0.24	0.27 ± 0.05

Free energies and m-values are in kcal.mol^{-1} and kcal.mol^{-1} M^{-1}, respectively. Confidence intervals (at the 95% level) are obtained by bootstrap analysis (1000 iterations), assuming parameter uncertainties to be normally distributed. The intrinsic free energy is represented as ΔG_X, where X indicates the type of repeat (N, R, W, C; see Figure 1 legend). The free energy of the interface between the repeats X-Y is represented as $\Delta G_{X\text{-}Y}$. Denaturant effects are modeled with a single intrinsic m-value (m_i), and a single interfacial m-value ($m_{i,i+1}$), regardless of the repeat sequence (N, R, W, C).

long-range coupling free energy, and decompose each term into enthalpy, entropy, heat capacity, and denaturant sensitivity. These parameters provide insight into bonding (ΔH), configurational restriction (ΔS), hydrophobic solvation (ΔC_p, along with ΔH and ΔS compensation) (Prabhu and Sharp, 2005), and burial of surface area (m-value).

Owing to their linear, repetitive architecture, the stability of repeat proteins and their high folding cooperativity can be described using a one-dimensional nearest-neighbor Ising model (Kajander et al., 2005; Mello and Barrick, 2004; Wetzel et al., 2008). In contrast to the simple systems traditionally analyzed with the Ising formalism, repeat proteins comprise all of the structural elements found in globular proteins, including hydrogen-bonded secondary structure (helix, turn, and sheet, depending on the type of repeat), burial and packing of nonpolar side chains, and charge interactions among surface groups (Kloss et al., 2008), and thus have direct relevance to nonrepeat (globular) proteins. In contrast to natural sequence-variable repeat proteins, synthetic repeat proteins with identical repeats can be represented with a limited set of parameters, decreasing the number of unknowns that must be extracted from experimental data. For a "homopolymer" with identical repeats, just two sets of parameters are needed (ΔG_i and $\Delta G_{i,i+1}$, along with associated denaturant and thermal parameters). Because a repeat protein array of n repeats has n-1 interfaces, ΔG_i and $\Delta G_{i,i+1}$ can be resolved by comparing the stabilities of a small number of constructs of different length (in principal, as few as two). However, the need to substitute polar residues on the termini to provide solubility introduces additional parameters, and thus, additional unknowns. Experimental resolution of these additional unknowns is facilitated by inclusion of constructs that lack one or the other capping repeat. This can be seen by representing constructs of different lengths as a system of linear equations (Equation S1) (Aksel and Barrick [2009]).

Free Energies of Intrinsic Folding, Interfacial Interaction, and Global Cooperativity

Comparing the free energies of intrinsic folding and interfacial interaction provides a unique means to quantify cooperativity in protein folding. High cooperativity should result from both favorable interfacial interactions and unfavorable intrinsic folding. We find both of these conditions to be met: at pH 8.0 and 5.0, interfacial interaction free energies to be stabilizing by 11–12.5 kcal/mol, whereas intrinsic folding free energies are +4 to +8 kcal/mol, depending on pH and repeat identity.

One way to represent these two components of cooperativity is as a difference, or "mismatch." The energy mismatch here (intrinsic minus interfacial) is around 15–17 kcal/mol per repeat,

which is reasonably close to the mismatch determined by Pluckthun et al. for an array of capped consensus ankyrin repeats (17.5–13.7 kcal/mol) (Wetzel et al., 2008). This mismatch is consistent with the high level of cooperativity observed experimentally. This mismatch is significantly larger than that observed in an experimental study of consensus TPR unfolding (Kajander et al., 2005). Like ankyrin repeats, TPR repeats have two antiparallel helices, although the sequence, helix lengths, turn structures, and interhelical geometries differ considerably. On a single-helix level, the intrinsic/interfacial energy mismatch is only 6.8 kcal/mol (+2.3 and −4.5 kcal/mol for intrinsic folding and interfacial interaction, respectively) (Kajander et al., 2005).

Effects of Sequence and pH Variation on Intrinsic and Interfacial Stability

Both at pH 8 and pH 5, $\Delta G_R < \Delta G_N < \Delta G_C$, spanning a range of 2.5 kcal/mol (Tables 3 and 4). Thus, our cap substitution decreases stability. Although we cannot analytically resolve these capping effects into intrinsic versus interfacial terms (Equations S2 and S3), we can resolve the intrinsic versus interfacial effects of trp substitution at position five. The stabilization seen by W repeats results from a decrease in intrinsic folding free energy by ~1.8 kcal/mol per repeat, which is modestly offset by a slight increase in interfacial interaction energy (0.7 kcal/mol) (Table 3).

The decrease in stability seen as the pH is lowered from 8 to 5 results primarily from an increase in the interfacial interaction energy (+1.9 kcal/mol) (Tables 3 and 4). There is a smaller, uniform increase in the intrinsic folding free energy (0.73, 0.78, and 0.77 kcal/mol for the N, R, and C repeats). Because the effect of pH in this range is likely to be linked to histidine ionization (two per N, R repeat; three in the C repeat), we expect the charged form of one or both histidines to weaken interactions between repeats, perhaps through electrostatic repulsion among these basic repeats (predicted pI of 9.52 for R).

Resolution of Cooperativity into Entropy, Enthalpy, and Heat Capacity Terms

The observation that intrinsic folding is entropically unfavorable (Table 4) suggests a loss of backbone configurational degrees of freedom. Along with a compensating favorable enthalpy change (Table 4), a significant unfavorable GdnHCl term (Table 3) suggests formation of native α-helical structure in the intrinsic folding step. Thermodynamic studies of monomeric α helices have shown helix formation to be enthalpically favorable, entropically unfavorable (Scholtz et al., 1991), and destabilized by GdnHCl (Smith and Scholtz, 1996).

The observation that interfacial interaction is entropically favorable but enthalpically unfavorable at low temperature
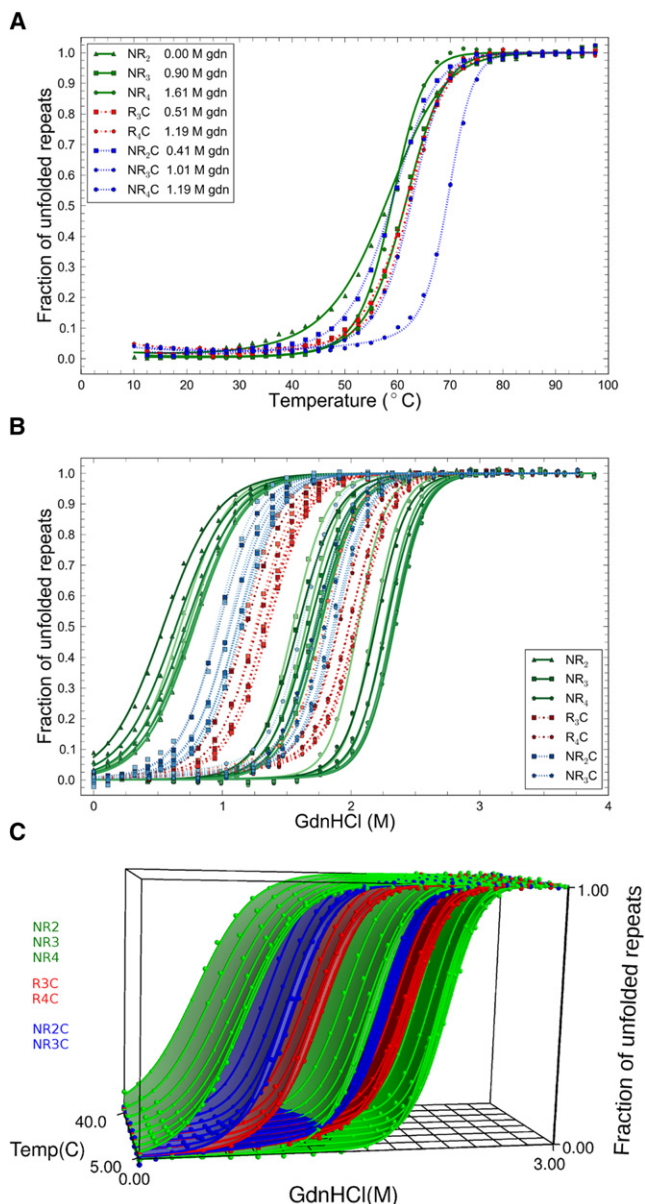
Figure 5. Temperature Dependence of Consensus Ankyrin Repeat Unfolding

(A) Thermal denaturation of CARPs in varying amounts of GdnHCl (see legend).

(B) GdnHCl titrations at different temperatures. Lines result from global fits, with $m_{i,i+1}/m_i = 0.5$. For each construct (legend) there are eight GdnHCl titrations performed at 5°C, 10°C, 15°C, 20°C, 25°C, 30°C, 35°C, and 40°C (increasing color from 5°C to 40°C).

(C) Three-dimensional representation of the temperature and GdnHCl dependence of CARP folding.

Curves in (A) and (B) and surfaces in (C) result from global Ising analysis as a function of temperature and GdnHCl, with $m_{i,i+1}/m_i = 0.5$. Surfaces in (C) are, from left to right, NR₂, NR₂C, R₃C, NR₃, NR₃C, R₄C, and NR₄. Conditions: 150 mM NaCl, 25 mM NaOAc (pH 5.0). To compare reversibility and structure at pH 8.0 and 5.0, see Figure S3.

(20°C) suggests a decrease in solvation of nonpolar groups. Hydrophobic desolvation at low temperature is favored by a large entropy increase that is partly offset by an enthalpy increase

(Baldwin, 1986; Privalov and Gill, 1988). A hallmark of the hydrophobic effect is a large decrease in heat capacity upon desolvation. The observation that the ΔC_p decrease seen for CARP folding is partitioned entirely into interfacial interaction suggests that hydrophobic groups are desolvated in this second step. The NMR structure of NRC shows substantial burial of nonpolar surface area between adjacent repeats (Figure 4C).

The interfacial interaction parameter provides long-range coupling and is critical for cooperative folding. The experimentally observed partitioning of hydrophobic desolvation into the interfacial interaction step indicates that hydrophobicity makes an important contribution to cooperativity in protein folding. However, we expect the interface formation to involve close packing, in addition to hydrophobic desolvation. Like nonpolar desolvation, interfacial packing is likely to involve long-range contacts distributed over many residues, consistent with cooperativity. In molten globule states of proteins, in which nonpolar surfaces are desolvated in the absence of rigid packing interactions, folding cooperativity is decreased. Simulation suggests that both hydrophobic desolvation and packing may contribute to cooperativity in folding (Kaya and Chan, 2003; Liu and Chan, 2005).

Using the NMR structure of NRC as a template, we generated structural models for longer constructs, and used these models to estimate solvent-accessible surface area (SASA)-based ΔH, ΔS, and ΔC_p values for unfolding (Hilser et al., 2006). Assuming linear additivity of intrinsic and interfacial terms, we resolved these energy terms into intrinsic and interfacial components (Table 4). The resulting SASA-based terms agree surprisingly well with experimental values. Most notably, intrinsic folding is entropically unfavorable, due in large part to conformational entropy decrease, whereas interfacial interaction is entropically driven, due largely to favorable desolvation. Also consistent with our findings, the heat capacity decrement is largely interfacial (Table 4).

Free-Energy Landscapes with Entropic and Enthalpic Resolution

Using the fitted energy terms from Ising analysis (Table 3), folding free-energy landscapes can be depicted in quantitative detail (Mello and Barrick, 2004; Tripp and Barrick, 2008; Wetzel et al., 2008). The free-energy landscape for NR₃C is shown in Figure 6A. Because the N- and C-terminal caps are less stable than the internal consensus repeats, partly folded conformations involving the central repeats have lower energy than conformations with structured termini, imparting a slightly concave shape from left to right. As with other repeat proteins analyzed in this way (Kloss et al., 2008; Mello and Barrick, 2004), favorable interfacial interactions tip the landscape toward the native state, once folding advances from a high energy point involving a single-folded repeat.

Decomposition of the intrinsic and interfacial terms into entropy, enthalpy, and heat capacity provides a more fundamental description of the progress of folding (Figures 6B and 6C). At 20°C, the folding enthalpy decreases (becomes more negative, relative to the unfolded state) as folding progresses (Figure 6B). This enthalpy decrease is substantial in the first step (folding a single repeat) but is smaller in subsequent steps of folding (folding paired with interaction with a structured neighbor). Overall, the reaction is enthalpy driven, but this drive

Table 4. Parameters from Temperature-Dependence Studies of Consensus Ankyrins at pH 5, 20°C

	$m_{i,i+1}/m_i = 0$	$m_{i,i+1}/m_i = 0.5$[a]	$m_{i,i+1}/m_i = 1$	$m_{i,i+1}/m_i = 10$	SASA-Based Energies[b]	
					Desolvation	Conformational
ΔG_N	6.86 ± 0.06	7.33 ± 0.06	7.59 ± 0.06	8.35 ± 0.07	8.4 ± 0.1	
ΔG_R	6.02 ± 0.05	6.50 ± 0.05	6.76 ± 0.06	7.52 ± 0.07	10.9 ± 0.1	
ΔG_C	8.52 ± 0.06	9.00 ± 0.07	9.27 ± 0.07	10.05 ± 0.11	10.7 ± 0.1	
$\Delta G_{i,i+1}$	−10.66 ± 0.11	−11.28 ± 0.10	−11.64 ± 0.11	−12.65 ± 0.12	−12.1 ± 0.1	
ΔS_i	−41.6 ± 4.9	−41.0 ± 5.2	−40.2 ± 5.4	−38.8 ± 5.9	54 ± 0.6	−121 ± 0.3
$\Delta S_{i,i+1}$	56.0 ± 7.1	55.1 ± 7.4	53.9 ± 7.7	51.9 ± 8.4	125 ± 0.6	−67 ± 0.3
$\Delta C_{p;\,i}$	−51 ± 71	23 ± 73	60 ± 82	191 ± 95	−113 ± 5.6	
$\Delta C_{p;\,i,i+1}$	−330 ± 102	−420 ± 104	−470 ± 117	−640 ± 135	−379 ± 5.6	
m_i	1.01 ± 0.01	0.73 ± 0.01	0.57 ± 0.00	0.12 ± 0.00	NA	
m_i^S	2.1 ± 0.5	1.6 ± 0.3	1.3 ± 0.3	0.3 ± 0.1	NA	
m_i^C	−50 ± 8	−38 ± 6	−30 ± 5	−6 ± 1	NA	
χ^2	8.11×10^{-5}	8.75×10^{-5}	9.31×10^{-5}	11.70×10^{-5}	NA	

Free energies are in kcal·mol^{-1}; entropies and heat capacities are in cal·mol^{-1}·K^{-1}; m-values are in kcal·mol^{-1}·M^{-1}; m_i^S and m_i^C are in cal·mol^{-1}·M^{-1}·K.

In each column, the $m_{i,i+1}/m_i$ ratio has been fixed to the indicated value to better constrain the fit. Confidence intervals are the results of 5000 iterations of bootstrap analysis, as described in Table 3. For population plots based on fitted parameters, see Figure S4.

[a] The $m_{i,i+1}/m_i$ ratio obtained from GdnHCl titration experiments at pH 8.0, 20°C.

[b] SASA-based ΔH, ΔS$_{conf}$, ΔS$_{solv}$, and ΔC$_p$ values were calculated from SASAs using parameters described in Hilser et al. (2006), using the NRC NMR structure determined here to calculate native-state SASA values for models of NR$_x$, NR$_y$C, and R$_y$C (x = 1–4; y = 2–4). Intrinsic and interfacial values were obtained by least squares fitting, assuming additivity (Aksel & Barrick, 2009). Uncertainties are least squares estimates.

comes largely from the first step (at 20°C, the last steps are enthalpically opposed as a result of cap substitutions). With the exception of the first step, where entropy strongly opposes folding, entropy increases with each folding/interface formation step. Thus, although there is an early entropy bottleneck at low temperature, folding is driven by entropy increase (Figure 6B) from solvent displacement from the interface.

Because of the large heat capacity decrease upon folding, this picture changes at higher temperatures. At 84°C, the T$_m$ for NR$_3$C (Figure 6C), entropy and enthalpy compensate one another. In the first step in folding, a destabilizing entropy decrease exceeds a stabilizing enthalpy decrease. As before, folding of a single repeat is disfavored. In subsequent steps the enthalpy decrease is greater (more stabilizing) than the entropy decrease, decreasing the overall free energy. This higher temperature picture is equivalent to analysis of funneled models for folding at T$_f$, and as predicted, imperfect enthalpy-entropy compensation gives rise to a cooperative two-state folding as a result of an entropy barrier (Go, 1983; Oliveberg and Wolynes, 2005; Onuchic et al., 2000; Taketomi et al., 1975; Thirumalai and Hyeon, 2005).

Although the current study is, to our knowledge, the first experimental decomposition of intrinsic and interfacial ΔH, ΔS, and ΔC$_p$ values for repeat protein folding, a simulation using a Go model of consensus TPR unfolding has been analyzed using an Ising-type framework (Ferreiro et al., 2008). Like the present study at high temperature, this simulation suggested intrinsic folding to be entropically opposed but enthalpically favored, although the lack of solvent in the simulation precludes detailed comparison. The interfacial interaction energy was only modeled to involve an enthalpic component (Ferreiro et al., 2008); whether the large interfacial entropy change identified here is specific to ankyrin versus TPR repeats,

or simply reflects the lack of solvent in the simulations, remains to be seen.

The Effect of Denaturant on Cooperativity

Although the free-energy mismatch described above is consistent with high cooperativity in the absence of denaturant, GdnHCl could diminish cooperativity if its effect was interfacial. In contrast we find that the fitted m$_i$-value is to be twice the m$_{i,i+1}$-value (Table 3), suggesting a further *enhancement* of cooperativity by GdnHCl in the transition region. GdnHCl preferentially destabilizes isolated folded repeats and, to a lesser extent, small clusters of folded repeats, which have higher repeat/interface ratios than fully folded CARPs.

To further explore the extent of cooperativity through the GdnHCl-unfolding transition, we used fitted Ising parameters to calculate the populations of partly folded states as a function of GdnHCl concentration (Figure S4). Although similar plots have been made for denaturant-induced unfolding of other repeat protein arrays (Mello and Barrick, 2004; Wetzel et al., 2008), the analysis here is based on an experimentally determined partitioning of the denaturant dependence into intrinsic and interfacial stability. We find that for short constructs (three to five repeats), fully folded and unfolded conformations dominate, with populations of partly folded states remaining below 20% (Figure S4). However, for longer constructs, partly folded states populate significantly through the transition and are dominated by species with one or both caps unfolded (in particular, the C-terminal cap) (Figure S4). These partly folded states are formed, in part, as a result of the higher intrinsic instability of the capping repeats (Table 3), as is seen in the highly destabilized C-terminal cap of Pluckthun et al. (Yu et al., 2006).

Because of this end fraying, the unfolding transitions of longer constructs are predicted to show a broad pretransition around

Figure 6. Folding Free-Energy Landscape of NR₃C
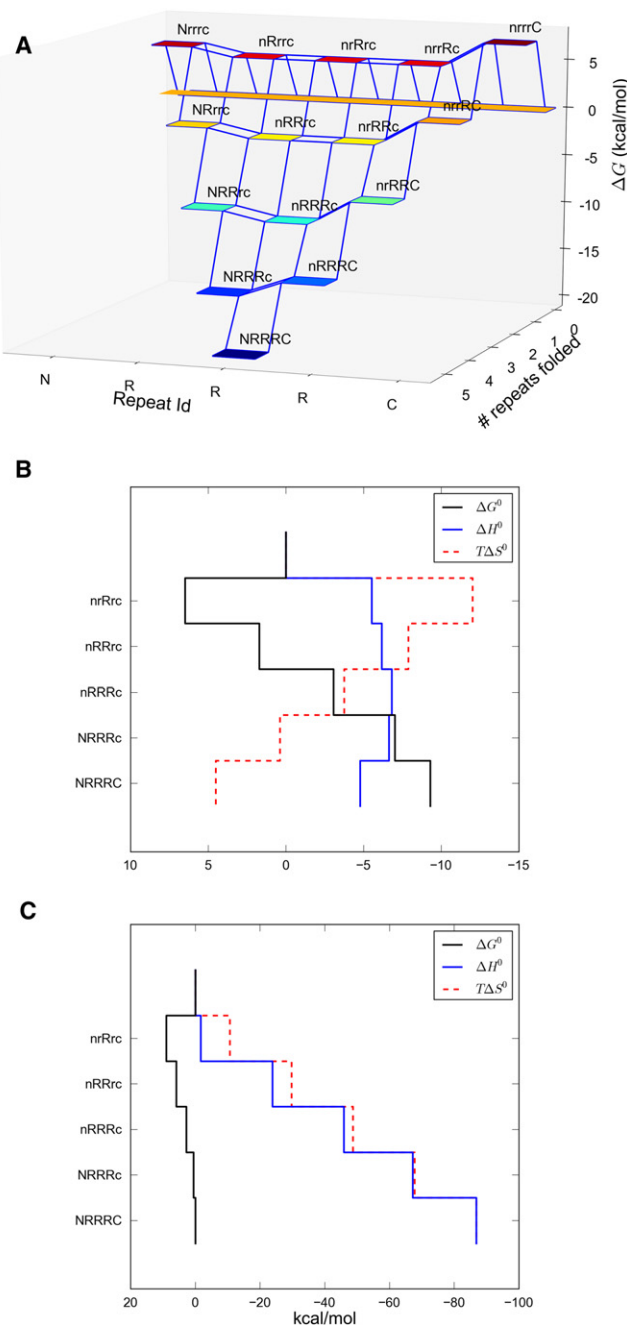
Figure 6. Folding Free-Energy Landscape of NR_3C

(A) Colored squares correspond to partially folded microstates. Folded and unfolded repeats are indicated using upper and lowercase letters, respectively (e.g., nrRRC has the N-cap and first R repeat unfolded, the last three repeats folded). Energies are calculated at 20°C in the absence of GdnHCl.

(B and C) Free energy, entropy, and enthalpy versus extent of folding (vertical). At low temperature (20°C; B), structuring the first repeat is unfavorable because it is entropically costly. When subsequent repeats are added, the array becomes stabilized, largely as a result of a favorable energy increase from interfacial pairing, but also because of a modest enthalpy decrease. At high temperature (T_m = 84°C; C), enthalpy and entropy compensate one another. This compensation is imperfect, such that the first repeats to fold are entropically destabilized more than they are enthalpically stabilized, rarifying partly folded states.

5–6 M GdnHCl, followed by a sharp transition at higher GdnHCl. To test this prediction we made CARPs containing nine and ten repeats (NR_7C and NR_8C) and monitored unfolding by GdnHCl titration. These longer constructs unfold extremely slowly, making equilibration difficult. By equilibrating samples for 2 days (Experimental Procedures), we were able to obtain unfolding curves quite close to equilibrium (Figure S4). As predicted from the Ising model, these curves show a pretransition from 5 to 6 M, followed by a sharp transition of greater amplitude. The minor differences (~0.2 M) between the midpoints of the major predicted and observed transitions may result from small errors in the fitted parameters, although we suspect incomplete equilibration to be a more likely contributor.

Although the methods used here to quantify the local and long-range interactions cannot be directly applied to globular proteins, the parameters determined here provide insight into globular protein stability. Partly folded structures of globular proteins that retain a subset of local interactions (e.g., secondary structures) will lose a disproportionate number of long-range interactions, even more than for the CARP substructures described here. Given the strong stabilizing long-range interactions found here, this would disproportionately destabilize partly folded structures. Native-state hydrogen exchange (NSHX) on globular proteins identifies such a stability gap between the native and partly unfolded states (intercepts in Figure 5 of Englander et al., 2002). This gap is critical for the observation, based on NSHX studies, that unfolding is highly cooperative through the GdnHCl transition despite a manifold of partly folded states with lower free energy than the denatured state (Englander et al., 2002).

EXPERIMENTAL PROCEDURES

Cloning, Expression, and Purification

CARP arrays were cloned as described in Supplemental Experimental Procedures and Figure S5. CARPS were expressed in BL21(DE3), and were purified as described in Supplemental Experimental Procedures.

Circular Dichroism Spectroscopy

All CD measurements were done using AVIV Model 400 CD spectrometer (Aviv Associates, Lakewood, NJ, USA). Far UV CD spectra were collected using a 1 mm path length quartz cuvette; protein concentrations ranged from 20 to 60 μM depending on construct size. At least three wavelength scans with 1 nm step size and 5 s averaging time were combined.

GdnHCl-Induced Unfolding Transitions at pH 8.0

GdnHCl-induced unfolding titrations were obtained using a Hamilton 500 titrator (Reno, NV, USA), and were monitored by CD at 222 nm. Protein concentrations ranged from 2 to 6 μM. Measurements were made in a silanized 1 cm quartz cuvette. Signal was averaged for 30 s at each step. To ensure full equilibration, a delay of several times the relaxation time (or a minimum of 180 s to ensure mixing) was introduced between GdnHCl injection and data acquisition. For NR_7C and NR_8C, relaxation times were too long for automated titration. Instead, individual samples were equilibrated at 20°C for 2 days prior to measurement.

To determine ΔG_i, $\Delta G_{i,i+1}$, m_i, and $m_{i,i+1}$, unfolding transitions of CARPS of different length and sequence composition were fitted globally to a heteropolymer Ising model using *Isingbul*, an in-house program for nearest neighbor analysis of protein denaturation data (unpublished data). Confidence intervals were determined at the 95% level by bootstrapping the residuals (see Aksel and Barrick, 2009).

Thermal and GdnHCl-Induced Unfolding Transitions at pH 5.0

Simple thermal denaturation experiments were performed in 1°C steps. For combined thermal/GdnHCl denaturation experiments, a single automated GdnHCl titration was generated in which the temperature was scanned (5°C increments) at each GdnHCl step. Equilibration times were decreased to minimize diffusion from the titrator tubing. Thermal melts were jointly fitted with GdnHCl melts at different temperatures using Isingbul, with a model that assumes that ΔG, ΔS, and ΔC_p vary linearly with GdnHCl (see Supplemental Experimental Procedures).

NMR Spectroscopy

^{15}N- and ^{15}N,^{13}C-labeled NRC was expressed and purified as described above, using M9 minimal media supplemented with ^{15}NH$_4$Cl and ^{13}C-labeled glucose (Cambridge Isotope Laboratories, Andover, MA, USA). Unless otherwise noted, NMR samples contained 2 mM NRC, 25 mM NaCl, 25 mM Na$_2$HPO$_4$, and 5% D$_2$O (pH 6.5). This pH maximized the number of well-resolved peaks in the ^{1}H,^{15}N-HSQC spectrum, presumably by decreasing exchange broadening of labile amide protons. For ^{13}C-edited 3D NOESY-HSQC experiments, ^{15}N,^{13}C-labeled NRC was lyophilized and redissolved in buffered D$_2$O (Cambridge Isotope Laboratories) at least three times to remove exchangeable amide protons. For RDC experiments, 0.5 mM NRC was aligned using a liquid crystalline medium containing 5% (by weight, relative to H$_2$O/D$_2$O) C12E6, with 1-hexanol (Sigma-Aldrich, St. Louis, MO, USA) at a mole ratio (to C12E6) of r = 0.64 (Rückertt and Otting, 2000).

Double- and triple-resonance spectra used to make resonance assignments are listed in Supplemental Experimental Procedures along with assignment methods, RDC measurement, structure determination, and ^{15}N-backbone dynamics.

ACCESSION NUMBERS

Assignments have been deposited in the BMRB (accession number 17306). Structural coordinates have been deposited in the PDB (accession number 2L6B).

SUPPLEMENTAL INFORMATION

Supplemental Information includes Supplemental Experimental Procedures, five figures, and one table and can be found with this article online at doi:10.1016/j.str.2010.12.018.

ACKNOWLEDGMENTS

REFERENCES

Aksel, T., and Barrick, D. (2009). Analysis of repeat-protein folding using nearest-neighbor statistical mechanical models. Methods Enzymol. *455*, 95–125.

Baldwin, R.L. (1986). Temperature dependence of the hydrophobic interaction in protein folding. Proc. Natl. Acad. Sci. USA *83*, 8069–8072.

Cervantes, C.F., Markwick, P.R., Sue, S.C., McCammon, J.A., Dyson, H.J., and Komives, E.A. (2009). Functional dynamics of the folded ankyrin repeats of I kappa B alpha revealed by nuclear magnetic resonance. Biochemistry *48*, 8023–8031.

DeLano, W.L. (2003). MacPyMOL: PyMOL Enhanced for Mac OS X (Palo Alto, CA: DeLano Scientific).

Doig, A.J. (2002). Recent advances in helix-coil theory. Biophys. Chem. *101-102*, 281–293.

Englander, S.W., Mayne, L., and Rumbley, J.N. (2002). Submolecular cooperativity produces multi-state protein unfolding and refolding. Biophys. Chem. *101-102*, 57–65.

Ferreiro, D.U., Walczak, A.M., Komives, E.A., and Wolynes, P.G. (2008). The energy landscapes of repeat-containing proteins: topology, cooperativity, and the folding funnels of one-dimensional architectures. PLoS Comput. Biol. *4*, e1000070.

Finn, R.D., Tate, J., Mistry, J., Coggill, P.C., Sammut, S.J., Hotz, H.R., Ceric, G., Forslund, K., Eddy, S.R., Sonnhammer, E.L., and Bateman, A. (2008). The Pfam protein families database. Nucleic Acids Res. *36*, D281–D288.

Go, N. (1983). Theoretical studies of protein folding. Annu. Rev. Biophys. Bioeng. *12*, 183–210.

Heinig, M., and Frishman, D. (2004). STRIDE: a web server for secondary structure assignment from known atomic coordinates of proteins. Nucleic Acids Res. *32*, W500–W502.

Hilser, V.J., Garcia-Moreno, E.B., Oas, T.G., Kapp, G., and Whitten, S.T. (2006). A statistical thermodynamic model of the protein ensemble. Chem. Rev. *106*, 1545–1558.

Ising, E. (1925). Beitrag zur Theorie des Ferromagnetismus. Z. Phys. A At. Nucl. *31*, 253–258.

Kajander, T., Cortajarena, A.L., Main, E.R., Mochrie, S.G., and Regan, L. (2005). A new folding paradigm for repeat proteins. J. Am. Chem. Soc. *127*, 10188–10190.

Kaya, H., and Chan, H.S. (2003). Simple two-state protein folding kinetics requires near-levinthal thermodynamic cooperativity. Proteins *52*, 510–523.

Kloss, E., Courtemanche, N., and Barrick, D. (2008). Repeat-protein folding: new insights into origins of cooperativity, stability, and topology. Arch. Biochem. Biophys. *469*, 83–99.

Liu, Z., and Chan, H.S. (2005). Solvation and desolvation effects in protein folding: native flexibility, kinetic cooperativity and enthalpic barriers under iso-stability conditions. Phys. Biol. *2*, S75–S85.

Lumry, R., and Biltonen, R. (1966). Validity of the "two-state" hypothesis for conformational transitions of proteins. Biopolymers *4*, 917–944.

Main, E.R., Xiong, Y., Cocco, M.J., D'Andrea, L., and Regan, L. (2003). Design of stable α-helical arrays from an idealized TPR motif. Structure *11*, 497–508.

Mandel, A.M., Akke, M., and Palmer, A.G., 3rd. (1995). Backbone dynamics of *Escherichia coli* ribonuclease HI: correlations with structure and function in an active enzyme. J. Mol. Biol. *246*, 144–163.

Mello, C.C., and Barrick, D. (2004). An experimentally determined protein folding energy landscape. Proc. Natl. Acad. Sci. USA *101*, 14102–14107.

Mosavi, L.K., and Peng, Z.Y. (2003). Structure-based substitutions for increased solubility of a designed protein. Protein Eng. *16*, 739–745.

Mosavi, L.K., Minor, D.L., Jr., and Peng, Z.Y. (2002). Consensus-derived structural determinants of the ankyrin repeat motif. Proc. Natl. Acad. Sci. USA *99*, 16029–16034.

Munoz, V. (2001). What can we learn about protein folding from Ising-like models? Curr. Opin. Struct. Biol. *11*, 212–216.

Myers, J.K., Pace, C.N., and Scholtz, J.M. (1995). Denaturant m values and heat capacity changes: relation to changes in accessible surface areas of protein unfolding. Protein Sci. *4*, 2138–2148.

Nicholson, E.M., and Scholtz, J.M. (1996). Conformational stability of the *Escherichia coli* HPr protein: test of the linear extrapolation method and a thermodynamic characterization of cold denaturation. Biochemistry *35*, 11369–11378.

Oliveberg, M., and Wolynes, P.G. (2005). The experimental survey of protein-folding energy landscapes. Q. Rev. Biophys. *38*, 245–288.

Onsager, L. (1944). Crystal statistics. I. A two-dimensional model with an order-disorder transition. Phys. Rev. *65*, 117–149.

Onuchic, J.N., Nymeyer, H., Garcia, A.E., Chahine, J., and Socci, N.D. (2000). The energy landscape theory of protein folding: insights into folding mechanisms and scenarios. Adv. Protein Chem. *53*, 87–152.

Poland, D., and Scheraga, H.A. (1970). Theory of Helix-Coil Transitions in Biopolymers (New York: Academic Press).

Prabhu, N.V., and Sharp, K.A. (2005). Heat capacity in proteins. Annu. Rev. Phys. Chem. *56*, 521–548.

Privalov, P.L., and Gill, S.J. (1988). Stability of protein structure and hydrophobic interaction. Adv. Protein Chem. *39*, 191–234.

Renner, C., Baumgartner, R., Noegel, A.A., and Holak, T.A. (1998). Backbone dynamics of the CDK inhibitor p19(INK4d) studied by 15N NMR relaxation experiments at two field strengths. J. Mol. Biol. *283*, 221–229.

Robertson, A.D., and Murphy, K.P. (1997). Protein structure and the energetics of protein stability. Chem. Rev. *97*, 1251–1268.

Rückertt, M., and Otting, G. (2000). Alignment of biological macromolecules in novel nonionic liquid crystalline media for NMR experiments. J. Am. Chem. Soc. *122*, 7793–7797.

Scholtz, J.M., Qian, H., York, E.J., Stewart, J.M., and Baldwin, R.L. (1991). Parameters of helix-coil transition theory for alanine-based peptides of varying chain lengths in water. Biopolymers *31*, 1463–1470.

Shen, Y., Delaglio, F., Cornilescu, G., and Bax, A. (2009). TALOS+: a hybrid method for predicting protein backbone torsion angles from NMR chemical shifts. J. Biomol. NMR *44*, 213–223.

Smith, J.S., and Scholtz, J.M. (1996). Guanidine hydrochloride unfolding of peptide helices: separation of denaturant and salt effects. Biochemistry *35*, 7292–7297.

Taketomi, H., Ueda, Y., and Go, N. (1975). Studies on protein folding, unfolding and fluctuations by computer simulation. I. The effect of specific amino acid sequence represented by specific inter-unit interactions. Int. J. Pept. Protein Res. *7*, 445–459.

Thirumalai, D., and Hyeon, C. (2005). RNA and protein folding: common themes and variations. Biochemistry *44*, 4957–4970.

Tripp, K.W., and Barrick, D. (2007). Enhancing the stability and folding rate of a repeat protein through the addition of consensus repeats. J. Mol. Biol. *365*, 1187–1200.

Tripp, K.W., and Barrick, D. (2008). Rerouting the folding pathway of the Notch ankyrin domain by reshaping the energy landscape. J. Am. Chem. Soc. *130*, 5681–5688.

Weinkam, P., Zong, C., and Wolynes, P.G. (2005). A funneled energy landscape for cytochrome c directly predicts the sequential folding route inferred from hydrogen exchange experiments. Proc. Natl. Acad. Sci. USA *102*, 12401–12406.

Wetzel, S.K., Settanni, G., Kenig, M., Binz, H.K., and Pluckthun, A. (2008). Folding and unfolding mechanism of highly stable full-consensus ankyrin repeat proteins. J. Mol. Biol. *376*, 241–257.

Wishart, D.S., and Sykes, B.D. (1994). The 13C chemical-shift index: a simple method for the identification of protein secondary structure using 13C chemical-shift data. J. Biomol. NMR *4*, 171–180.

Yu, H., Kohl, A., Binz, H.K., Pluckthun, A., Grutter, M.G., and van Gunsteren, W.F. (2006). Molecular dynamics study of the stabilities of consensus designed ankyrin repeat proteins. Proteins *65*, 285–295.

Zimm, B.H. (1960). Theory of "Melting" of the helical form in double chains of the DNA type. J. Chem. Phys. *33*, 1349–1356.

Zweifel, M.E., and Barrick, D. (2002). Relationships between the temperature dependence of solvent denaturation and the denaturant dependence of protein stability curves. Biophys. Chem. *101-102*, 221–237.

Supplemental Information

The Contribution of Entropy, Enthalpy,

and Hydrophobic Desolvation to Cooperativity

in Repeat-Protein Folding

Tural Aksel, Ananya Majumdar, and Doug Barrick

Table S1, related to Figure 4. The statistics of the local models assigned in modelfree analysis

Model definition[a]	Number of Spins assigned[b]
Model 1 (S_s^2)	60
Model 2 (S_s^2, τ_e)	2 (19,24)
Model 3 (S_s^2, R_{ex})	8 (11, 17, 26, 39, 59, 61, 62, 94)
Model 4 (S_s^2, τ_e, R_{ex})	3 (6, 29, 92)
Model 5 (S_s^2, S_f^2, τ_e)	12 (7, 8, 9, 10, 32, 33, 96, 97, 99, 100, 101, 102)

[a]Each of five models evaluated for each NH includes, in addition to the global parameters in Table 2, a set of local parameters that are optimized individually (in parentheses) for each residue: S_s, order parameter on a slow time scale; S_f, order parameter on a fast time scale; τ_e, internal correlation time; R_{ex}, chemical exchange rate. [b]The identities of ^{15}N-^1H spins analyzed using a particular model are given in parenthesis.
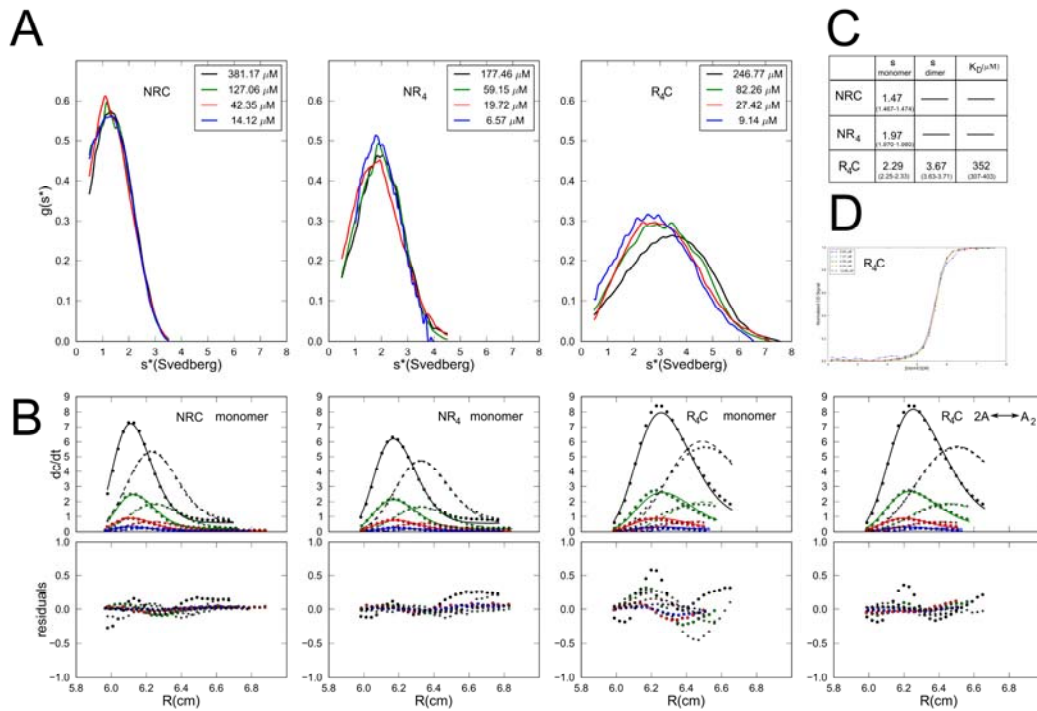
Figure S1, related to Figure 1.

Concentration dependence of sedimentation and GdnHCl unfolding transitions of CARPs (A) g(s*) plots from sedimentation velocity AUC at four different concentrations (see legend). (B) dc/dt data at the concentrations indicated in (A). Solid lines correspond to fits with a monomer or homodimer model. Only the first (filled circles) and last (stars) dc/dt curves are shown. NR_1C and NR_4 data are adequately described by the monomer model, whereas R_4C is best described by a homodimerization model. Both g(s*) and dc/dt analysis were performed using SEDANAL (Stafford and Sherwood, 2004). (C) Fitted parameters from dc/dt analysis. Errors were estimated from bootstrapping. Conditions: 150 mM NaCl, 25 mM Tris-Cl, pH 8.0, 20°C for NR_1C and NR_4; 1.2 M GdnHCl 150 mM NaCl, 25 mM Tris-Cl, pH 8.0, 20°C for R_4C. Samples were dialyzed extensively and were spun at 50,000 rpm in meniscus-matching cells (Spin Analytical, Durham NH), against the dialysis buffer. Concentration profiles were determined using interference optics. (D) GdnHCl unfolding transitions of R_4C are independent of concentration. Unfolding transitions were measured as described in the text, at protein concentrations given in the legend. Due to the slow unfolding kinetics around the midpoint of this large construct, equilibration times of 45 minutes were used in the transition region. Conditions: 150 mM NaCl, 25 mM Tris HCl, pH 8.0, 20°C.
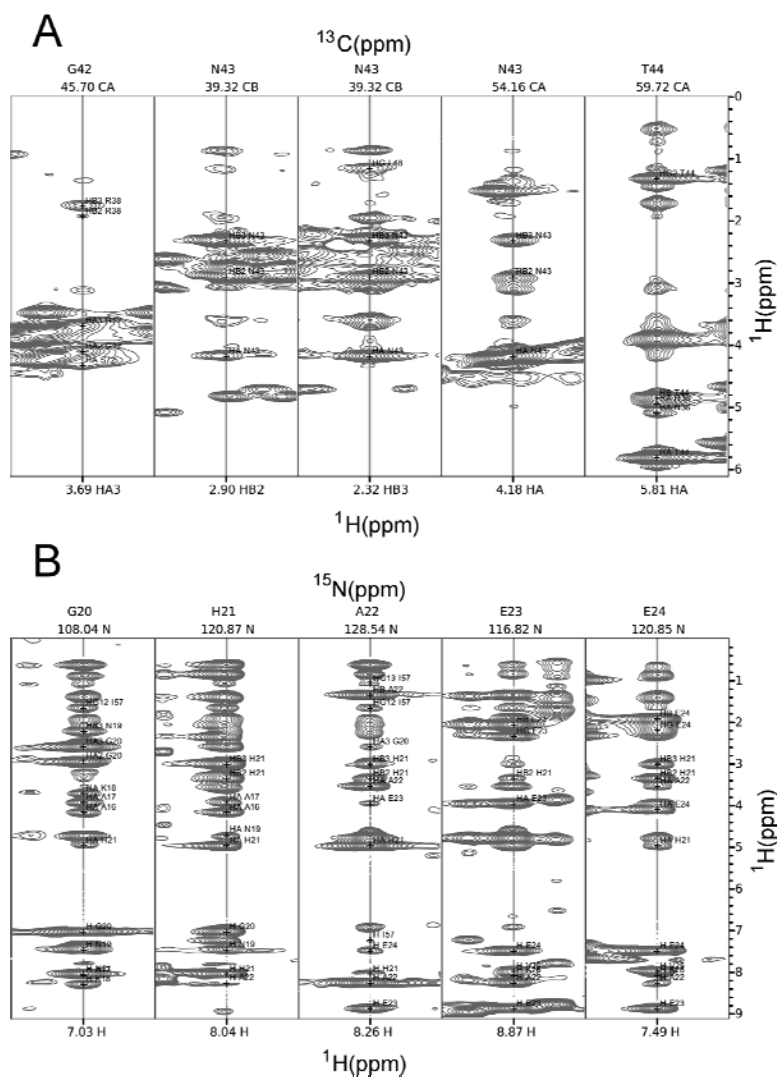
Figure S2, related to Figure 2. Representative strip plots from (A) ^{13}C-edited ^{1}H-^{1}H NOESY and (B) ^{15}N-edited ^{1}H-^{1}H NOESY spectra
Samples contained 2 mM ^{13}C- and ^{15}N-labelled NRC (A and B, respectively) at 600 MHz (pH 6.5, 25°C).
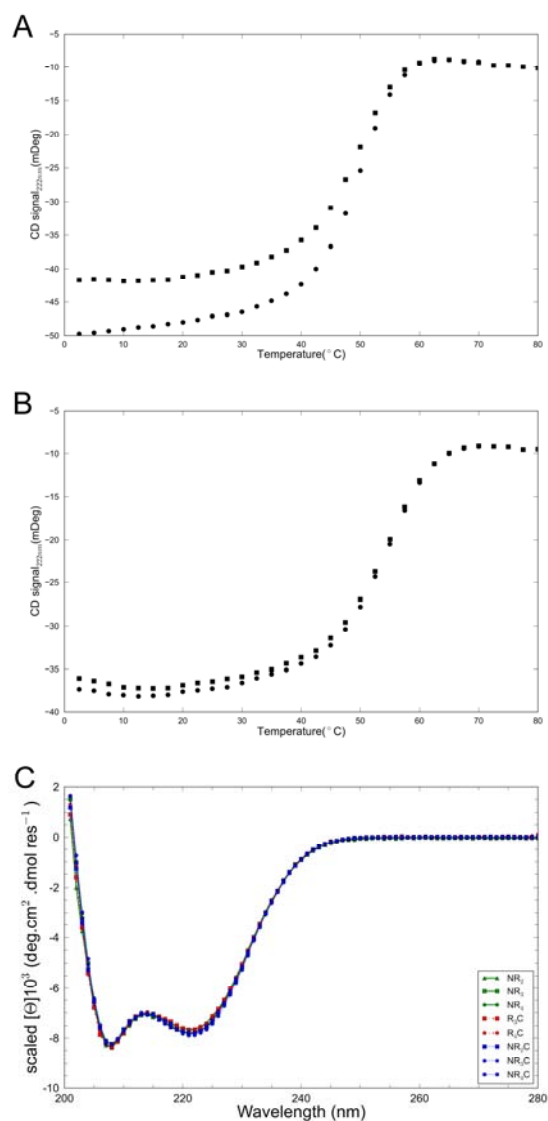
Figure S3, related to Figure 5. Reversibility of thermal denaturation of NR$_3$ at (A) pH 8.0 and (B) pH 5.0, and CD spectra at (C) pH 5.0

Reversibility is checked by measuring the recovery of native state CD signal observed at 222 nm following a jump to low temperature after a thermal denaturation experiment, and comparison of the shape of initial and subsequent unfolding transitions (circles and squares, respectively). Spectra are scaled as described in Figure 1. Conditions are (A) 4.2 M Gdn-HCl 150 mM NaCl, 25 mM Tris-HCl pH 8.0, 20 °C; (B) 1.18 M Gdn-HCl 150mM NaCl, 25 mM NaAc, pH 5.0; 150mM NaCl, 25 mM NaOAc, pH 5.0, 20 °C.
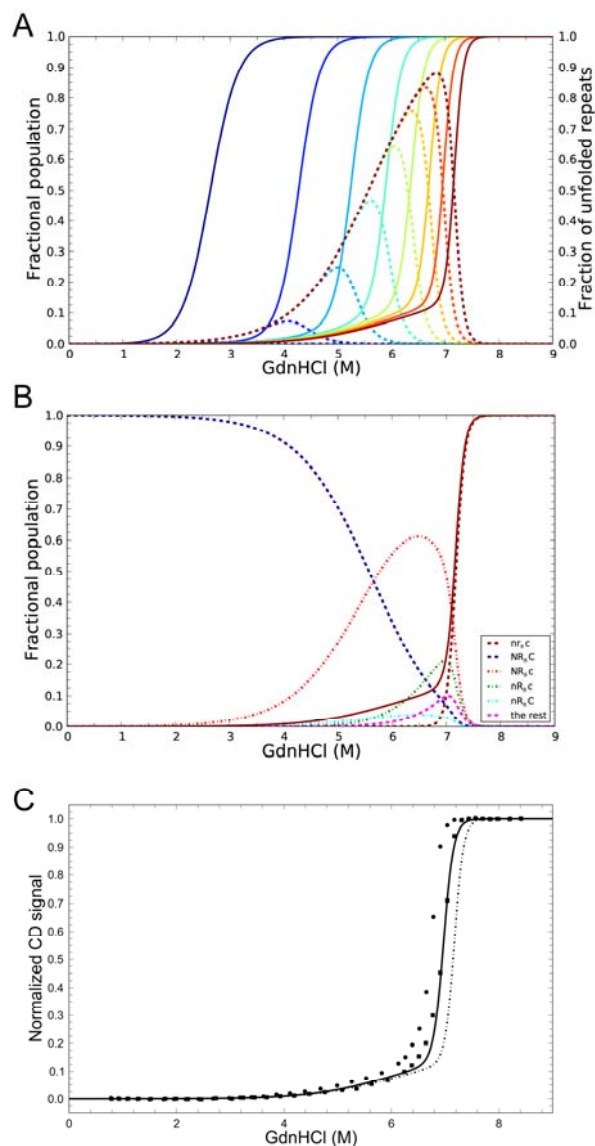
Figure S4, related to Table 4. Populations of folded, unfolded, and partly folded states in GdnHCl-induced unfolding transitions
(A) Simulated unfolding curves (solid lines) for constructs containing three (left, NRC) to ten repeats (right, NR_8C), and the total population of partly folded states (dashed lines, same color scheme as for the simulated unfolding curves). (B) Composition of partly folded species of NR_8C. The solid line gives the simulated unfolding curve. Dashed lines show the partly folded states that are most populated, along with the fully folded and fully unfolded states (see legend; upper and lower case represent folded and unfolded repeats respectively, "the rest" accounts for the remaining partly folded states not listed in the legend). (C) Manual GdnHCl titrations of NR_7C and NR_8C (circles and squares, respectively), and predicted unfolding transitions using fitted intrinsic and interfacial energies (solid and dashed lines, respectively). Conditions: 150 mM NaCl, 25 mM Tris•HCl, pH 8.0, $20°C$.
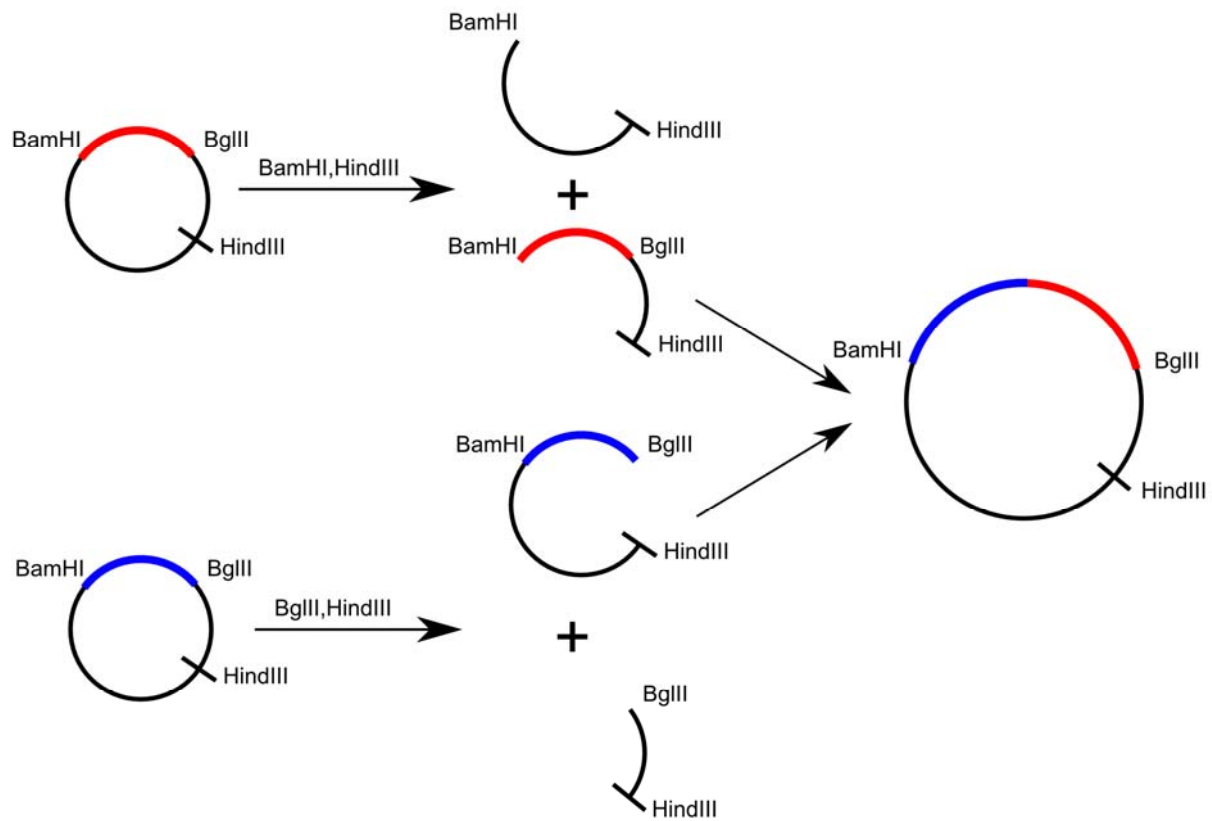
Figure S5, related to Table 1. Cloning scheme used to create CARP arrays from single repeats (or arrays)

Red and blue colored regions represent the ORFs encoding two different CARP arrays. The two plasmids were digested by different sets of restriction enzymes (red: *BamHI* and *HindIII;* blue: *BglII* and *HindIII*). Ligation of fragments containing the red and blue CARP-encoding segments expands the CARP array, retaining the flanking *BamHI* and *BglII* sites while eliminating the internal site.

Supplemental Experimental Procedures

Cloning of consensus ankyrin repeat proteins. To clone capped arrays of CARPS-encoding genes, oligonucleotides (IDT; Coralville, IA) encoding single consensus repeats were kinased and ligated into the *BamHI* and *BglII* sites of a modified pET15b expression vector (Novagen; Darmstadt, Germany) in which the *BglII* site was removed, a new *BglII* site was introduced adjacent to the *BamH1* site, and the N-terminal his$_6$ sequence was replaced with a C-terminal his$_6$-tag. Inserts encoding single repeats were then multimerized by ligating DNAs cut with a 3' (with respect to coding) *BglII* site to a 5' *BamHI* site, along with a distal *HindIII* site (Figure S5). The overhangs generated by *BamHI* and *BglII* digestion are cohesive, but their ligation eliminates both sites (Carrion-Vazquez et al., 1999). Repeating this second joining step results in geometric expansion of the CARP array, and also provides a means to add capping terminal capping repeats. Constructs were confirmed by restriction digestion and by DNA sequencing from both directions.

E. coli BL21(DE3) cells were transformed with plasmids containing CARP genes, and were grown in Terrific Broth (Tartoff and Hobbs, 1987) at 37°C to an OD$_{600}$ of 1.0. Expression was induced by addition of 1 mM IPTG. After further growth for 10 hours at 37°C, cells were collected by centrifugation and were frozen at -80°. Cells were resuspended in 300 mM NaCl, 50 mM Tris-HCl, pH 8.0, and were lysed with a french press. Lysate pellets were resuspended in 8M urea, 0.02% PEI, 200 mM NaCl, 50 mM Tris-HCl solution at pH 8.0, and were re-centrifuged to remove precipitated DNA. The supernatant was loaded onto a nickel column (QIAGEN; Valencia, CA). After washing with same denaturing solution, bound protein was refolded on the column by washing with 200 mM NaCl, 50 mM Tris-Cl, pH 8.0, and was eluted with 0.5 M imidazole, 200 mM NaCl, 50 mM Tris-Cl, pH 8.0. Protein-containing fractions were concentrated to ~5 mg/ml.

NMR spectroscopy, assignments, and structure determination. Double-(^{15}N-H and ^{13}C-H HSQC) and triple-resonance spectra (HNN, CBCA(CO)NH, HBHA(CO)NH, HNCACB, (H)CC(CO)NH, H(CC)(CO)NH, ^{15}N-edited HSQC-NOESY, ^{15}N-edited HMQC-NOESY-HSQC, ^{13}C-edited HSQC-NOESY, and ^{13}C-edited HMQC-NOESY-HSQC) used for backbone and side-chain assignments and for measurement of ^{1}H,^{1}H NOE's were obtained on a Bruker Avance II 600 MHz spectrometer equipped with a cryoprobe. Two sets of IPAP spectra in alignment media and in isotropic solution on a Varian Inova 800 MHz spectrometer equipped with a cryoprobe to obtain RDC values. Relaxation studies to determine values for R$_1$, R$_2$, and ^{1}H-^{15}N NOE's were performed at 600 MHz.

Data were processed using NMRPipe (Delaglio et al., 1995). Assignments and peak intensities were determined using CARA (Masse and Keller, 2005). NOE distance restraint determinations and structure calculations were performed using CYANA (Guntert, 2004) interfaced with UNIO (Herrmann et al., 2002). Structural models were further optimized against RDC data using XPLOR-NIH (Schwieters et al., 2003).

To explore backbone dynamics, ^{15}N-^{1}H correlation spectra were collected at 600 MHz; R$_1$, R$_2$ and ^{1}H-^{15}N NOE relaxation parameters were extracted using in-house scripts. The FASTModelFree interface (Cole and Loria, 2003) to modelfree (Mandel et al., 1995) was used to perform Lipari and Szabo's modelfree analysis. A global rotational correlation time (τ_m) of 7.86±0.02 ns, and a ratio of the axial and perpendicular rotational diffusion constants ($D_P/D_\perp$) of 1.42±0.03, were estimated from

the analysis. The statistical test described in (Mandel et al., 1995) was used to select the best dynamic model for each spin (see Table S1).

Analysis of CARP thermal unfolding transitions. To obtain the intrinsic and interfacial entropy, enthalpy and heat capacity changes (ΔS_i, $\Delta S_{i,i+1}$, ΔH_i, $\Delta H_{i,i+1}$ $\Delta C_{p;\ i}$, $\Delta C_{p;\ i,i+1}$), ΔG_i, $\Delta G_{i,i+1}$ are expressed as follows:

$$\Delta G^\circ_i(T) \ = \ \Delta G^\circ_i(T_r) + (T - T_r)\Delta C_{p;\ i} - (T - T_r)\Delta S^\circ_i - T\Delta C_{p;\ i}\ln\frac{T}{T_r}$$

$$\Delta G^\circ_{i,i+1}(T) \ = \ \Delta G^\circ_{i,i+1}(T_r) + (T - T_r)\Delta C_{p;\ i,i+1} - (T - T_r)\Delta S^\circ_{i,i+1} - T\Delta C_{p;\ i,i+1}\ln\frac{T}{T_r}$$

(2)

T_r, a constant of integration, serves as a reference temperature. Equation 2 assumes that the ΔC_p terms are independent of temperature.

The temperature dependences of the intrinsic and interfacial m-values are expressed in a form similar to Equation 2:

$$m^\circ_i(T) = m^\circ_i(T_r) + (T - T_r)\frac{d\Delta C_{p;\ i}}{dX} - (T - T_r)\frac{d\Delta S^\circ_i}{dX} - T\frac{d\Delta C_{p;\ i}}{dX}\ln\frac{T}{T_r}$$

$$= m^\circ_i(T_r) + (T - T_r)m^C_i - (T - T_r)m^S_i - Tm^C_i\ln\frac{T}{T_r}$$

(3)

$$m^\circ_{i,i+1}(T) = m^\circ_{i,i+1}(T_r) + (T - T_r)\frac{d\Delta C_{p;\ i,i+1}}{dX} - (T - T_r)\frac{d\Delta S^\circ_{i,i+1}}{dX} - T\frac{d\Delta C_{p;\ i,i+1}}{dX}\ln\frac{T}{T_r}$$

$$= m^\circ_{i,i+1}(T_r) + (T - T_r)m^C_{i,i+1} - (T - T_r)m^S_{i,i+1} - Tm^C_{i,i+1}\ln\frac{T}{T_r}$$

where X is the molar GdnHCl concentration. Equation 3 is obtained by partial differentiation of Equation 2 with respect to denaturant concentration (e.g., $m_i = \left(\partial\Delta G_i/\partial X\right)_T$ for the intrinsic interaction). In the second line of each equality in Equation 3, m^S and m^C are shorthand for the denaturant derivatives of entropy and heat capacity. For simplicity, we assume ΔC_p and ΔS° to have a linear GdnHCl dependence, making m^S and m^C constant. This is justified in part by the often-observed linearity of ΔG with denaturant concentration, and in part by the linear dependence of ΔC_p on denaturant concentration for the ankyrin domain of the Notch receptor (Zweifel and Barrick, 2002).

Equations 2 and 3 can be combined to give expressions for ΔG_i and $\Delta G_{i,i+1}$ as a function of denaturant concentration:

$$\Delta G°_i(T,X) = \Delta G°_i(T,X=0) - m_i(T)X$$
$$\Delta G°_{i,i+1}(T,X) = \Delta G°_{i,i+1}(T,X=0) - m_{i,i+1}(T)X \tag{4}$$

Equations 2-4 were globally fitted to thermal and GdnHCl unfolding transitions, in triplicate, for constructs of different length and composition (64 curves total), using bootstrap analysis of residuals to estimate 95 percent confidence intervals on fitted parameters (Table 4).

Matrix representation of nearest-neighbor models for repeat protein folding. Because the linear Ising model represents the free energy of folded repeat proteins additively, a system of repeat proteins and their measured free energies of unfolding can be regarded as a set of linear equations. These equations can be expressed compactly in matrix form, is shown in Equation S1:

$$
\begin{pmatrix}
1 & 1 & 0 & 1 \\
1 & 2 & 0 & 2 \\
1 & 3 & 0 & 3 \\
1 & 4 & 0 & 4 \\
0 & 2 & 1 & 2 \\
0 & 3 & 1 & 3 \\
0 & 4 & 1 & 4 \\
1 & 1 & 1 & 2 \\
1 & 2 & 1 & 3 \\
1 & 3 & 1 & 4
\end{pmatrix}
\begin{pmatrix}
\Delta G^o_N \\
\Delta G^o_R \\
\Delta G^o_C \\
\Delta G^o_{i,i+1}
\end{pmatrix}
=
\begin{pmatrix}
\Delta G^o_{NR_1} \\
\Delta G^o_{NR_2} \\
\Delta G^o_{NR_3} \\
\Delta G^o_{NR_4} \\
\Delta G^o_{R_2C} \\
\Delta G^o_{R_3C} \\
\Delta G^o_{R_4C} \\
\Delta G^o_{NR_1C} \\
\Delta G^o_{NR_2C} \\
\Delta G^o_{NR_3C}
\end{pmatrix}
\tag{1}
$$

These equations describe stabilities of ten constructs including N- and C- caps and internal repeats R (but no W-substituted repeats). The vector on the right-hand-side of Equation (S1) represents the (observable) folding free energies of each construct, relative to the denatured state. The vector on the left-hand side represents the intrinsic and interfacial free energy terms (unknowns), and the coefficient matrix gives the number of repeats of each type and the total number of interfaces for each construct. Inspection of the coefficient matrix on the left-hand side shows each column to be independent of the other three: no column can be obtained by linear combination of any of the other three columns (i.e., the matrix has full column rank, $r=4$). Thus, within the framework of this four-parameter model, these equations (S1) may be expected to have a unique solution (at least in the least-squares limit, allowing for errors in the measured free energy vector).

Although we obtain optimized parameters by fitting the full partition function to unfolding transitions, the representation illustrated by Equation (S1) provides a simple way to test whether the unknown parameters of a particular energy model can be extracted from a given set of constructs. For example, matrix representation of a model that includes separate terms for the interfaces between the capping (N and C) repeats and the internal (R) repeats can be written as

$$
\begin{pmatrix}
1 & 1 & 0 & 0 & 1 & 0 \\
1 & 2 & 0 & 1 & 1 & 0 \\
1 & 3 & 0 & 2 & 1 & 0 \\
1 & 4 & 0 & 3 & 1 & 0 \\
0 & 2 & 1 & 1 & 0 & 1 \\
0 & 3 & 1 & 2 & 0 & 1 \\
0 & 4 & 1 & 3 & 0 & 1 \\
1 & 1 & 1 & 0 & 1 & 1 \\
1 & 2 & 1 & 1 & 1 & 1 \\
1 & 3 & 1 & 2 & 1 & 1
\end{pmatrix}
\begin{pmatrix}
\Delta G^o_N \\
\Delta G^o_R \\
\Delta G^o_C \\
\Delta G^o_{R,R} \\
\Delta G^o_{N,R} \\
\Delta G^o_{R,C}
\end{pmatrix}
=
\begin{pmatrix}
\Delta G^o_{NR_1} \\
\Delta G^o_{NR_2} \\
\Delta G^o_{NR_3} \\
\Delta G^o_{NR_4} \\
\Delta G^o_{R_2C} \\
\Delta G^o_{R_3C} \\
\Delta G^o_{R_4C} \\
\Delta G^o_{NR_1C} \\
\Delta G^o_{NR_2C} \\
\Delta G^o_{NR_3C}
\end{pmatrix}
\qquad (S2)
$$

This system can easily be seen to lack a unique solution. The new columns introduced to the coefficient matrix would be identical to columns 1 and 3 above; thus, Gaussian elimination knocks out the six bottom equations from the system in Equation S2:

$$
\begin{pmatrix}
1 & 1 & 0 & 0 & 1 & 0 \\
0 & 1 & 0 & 1 & 0 & 0 \\
0 & 0 & 1 & -1 & 0 & 1 \\
0 & 0 & 0 & 1 & 0 & 0 \\
0 & 0 & 0 & 0 & 0 & 0 \\
0 & 0 & 0 & 0 & 0 & 0 \\
0 & 0 & 0 & 0 & 0 & 0 \\
0 & 0 & 0 & 0 & 0 & 0 \\
0 & 0 & 0 & 0 & 0 & 0 \\
0 & 0 & 0 & 0 & 0 & 0
\end{pmatrix}
\qquad (S3)
$$

Thus, there are only four unique equations (and thus a column rank of four; this is the same as the rank in Equation S1, which is to be expected since it describes same set of constructs).

All of the models used here to describe CARP unfolding have a unique solution when cast using this matrix formalism.

Supplemental References

Carrion-Vazquez, M., Oberhauser, A.F., Fowler, S.B., Marszalek, P.E., Broedel, S.E., Clarke, J., and Fernandez, J.M. (1999). Mechanical and chemical unfolding of a single protein: a comparison. Proceedings of the National Academy of Sciences of the United States of America *96*, 3694-3699.

Cole, R., and Loria, J.P. (2003). FAST-Modelfree: a program for rapid automated analysis of solution NMR spin-relaxation data. Journal of biomolecular NMR *26*, 203-213.

Delaglio, F., Grzesiek, S., Vuister, G.W., Zhu, G., Pfeifer, J., and Bax, A. (1995). NMRPipe: a multidimensional spectral processing system based on UNIX pipes. Journal of biomolecular NMR *6*, 277-293.

Guntert, P. (2004). Automated NMR structure calculation with CYANA. Methods in molecular biology (Clifton, N.J *278*, 353-378.

Herrmann, T., Guntert, P., and Wuthrich, K. (2002). Protein NMR structure determination with automated NOE assignment using the new software CANDID and the torsion angle dynamics algorithm DYANA. Journal of molecular biology *319*, 209-227.

Mandel, A.M., Akke, M., and Palmer, A.G., 3rd (1995). Backbone dynamics of Escherichia coli ribonuclease HI: correlations with structure and function in an active enzyme. Journal of molecular biology *246*, 144-163.

Masse, J.E., and Keller, R. (2005). AutoLink: automated sequential resonance assignment of biopolymers from NMR data by relative-hypothesis-prioritization-based simulated logic. J Magn Reson *174*, 133-151.

Schwieters, C.D., Kuszewski, J.J., Tjandra, N., and Clore, G.M. (2003). The Xplor-NIH NMR molecular structure determination package. J Magn Reson *160*, 65-73.

Stafford, W.F., and Sherwood, P.J. (2004). Analysis of heterologous interacting systems by sedimentation velocity: curve fitting algorithms for estimation of sedimentation coefficients, equilibrium and kinetic constants. Biophysical chemistry *108*, 231-243.

Tartoff, K.D., and Hobbs, C.A. (1987). Improved media for growing plasmid and cosmid clones. Bethesda Research Laboratories Focus *9*.

Zweifel, M.E., and Barrick, D. (2002). Relationships between the temperature dependence of solvent denaturation and the denaturant dependence of protein stability curves. Biophysical chemistry *101-102*, 221-237.